Metabolic Engineering 52 (2019) 303–314

Contents lists available at ScienceDirect

Metabolic Engineering

journal homepage: www.elsevier.com/locate/meteng

Mapping *Salmonella typhimurium* pathways using ^{13}C metabolic flux analysis

Daniela M. Correia[a,1], Cintia R. Sargo[a,1], Adilson J. Silva[a,1], Sophia T. Santos[b], Roberto C. Giordano[a], Eugénio C. Ferreira[b], Teresa C. Zangirolami[a], Marcelo P.A. Ribeiro[a], Isabel Rocha[b,c,*]

[a] Graduate Program of Chemical Engineering, Federal University of São Carlos, Rodovia Washington Luís, Km 235, São Carlos, SP 13565-905, Brazil
[b] CEB—Centre of Biological Engineering, University of Minho, Campus De Gualtar, Braga 4710-057, Portugal
[c] Instituto de Tecnologia Química e Biológica António Xavier, Universidade Nova de Lisboa (ITQB-NOVA), Oeiras, Portugal

ARTICLE INFO

Keywords:
Salmonella typhimurium
Chemostat culture
^{13}C-MFA
Genome-scale metabolic model
In silico simulation

ABSTRACT

In the last years, *Salmonella* has been extensively studied not only due to its importance as a pathogen, but also as a host to produce pharmaceutical compounds. However, the full exploitation of *Salmonella* as a platform for bioproduct delivery has been hampered by the lack of information about its metabolism. Genome-scale metabolic models can be valuable tools to delineate metabolic engineering strategies as long as they closely represent the actual metabolism of the target organism. In the present study, a ^{13}C-MFA approach was applied to map the fluxes at the central carbon pathways of *S. typhimurium* LT2 growing at glucose-limited chemostat cultures. The experiments were carried out in a 2L bioreactor, using defined medium enriched with 20% ^{13}C-labeled glucose. Metabolic flux distributions in central carbon pathways of *S. typhimurium* LT2 were estimated using OpenFLUX2 based on the labeling pattern of biomass protein hydrolysates together with biomass composition. The results suggested that pentose phosphate is used to catabolize glucose, with minor fluxes through glycolysis. *In silico* simulations, using Optflux and pFBA as simulation method, allowed to study the performance of the genome-scale metabolic model. In general, the accuracy of *in silico* simulations was improved by the superimposition of estimated intracellular fluxes to the existing genome-scale metabolic model, showing a better fitting to the experimental extracellular fluxes, whereas the intracellular fluxes of pentose phosphate and anaplerotic reactions were poorly described.

1. Introduction

Salmonella enterica serovar Typhimurium (*S. typhimurium*) is an intracellular mammalian pathogen that belongs to the *Enterobacteriaceae* family. Several studies addressing virulence, pathogenicity, host-microbe interactions, and genetics of *S. typhimurium* have been published (Dandekar et al., 2012, 2015; Kaufmann et al., 2001). Besides the recognized importance as a pathogen itself, in the last years, *Salmonella* has gained increasing attention in the biotechnological area as a potential host to produce several pharmaceutical compounds (Silva et al., 2014). Among the products that can be produced with *Salmonella typhimurium* are flagellin, capsular polysaccharide Vi, lipopolysaccharides, and vaccines, with applications in human and veterinary medicine (Braga et al., 2010; Kong et al., 2013; Kothari et al., 2014; Oliveira et al., 2011). Attenuated strains of *Salmonella* are being used as Live Bacterial Vectors (LBV), for immunization against itself or to deliver heterologous antigens (Silva et al., 2014). In addition, promising results have been obtained with the utilization of *Salmonella* in treatment and vaccination against non-infectious diseases, such as several types of cancer, including melanoma, and breast, prostate, pancreatic and cervix cancers (Bolhassani and Zahedifard, 2012; Forbes, 2010; Heimann and Rosenberg, 2003).

Metabolic engineering has been applied, with success, in genetic improvement of a variety of organisms. Through the rational selection of gene targets to be manipulated, it is possible, for instance, to improve the production of a given molecule or to reduce the secretion of an undesirable metabolite (Stephanopoulos et al., 1998). To this end, genome-scale metabolic models are important tools that allow predicting phenotypes under different conditions, supporting the development of metabolic engineering strategies. Another important application of genome-scale metabolic models is the identification of metabolic drug targets, with a possible relevant contribution in fighting

* Corresponding author at: Instituto de Tecnologia Química e Biológica António Xavier, Universidade Nova de Lisboa (ITQB-NOVA), Oeiras, Portugal.
E-mail address: irocha@itqb.unl.pt (I. Rocha).
[1] These authors contributed equally to this work.

https://doi.org/10.1016/j.ymben.2018.11.011
Received 19 March 2018; Received in revised form 26 November 2018; Accepted 28 November 2018
Available online 04 December 2018

Salmonella infections (Hartman et al., 2014). To achieve these goals, the simulations obtained with metabolic models must have high accuracy, which is only possible through the knowledge and understanding of the organism's metabolism.

For *S. typhimurium* LT2 there are four genome-scale metabolic models available in the literature (Abuon et al., 2009; Raghunathan et al., 2009; Thiele et al., 2011; Hartman et al., 2014). However, all present a low degree of experimental validation, due to the lack of experimental data for *Salmonella typhimurium* LT2 obtained under controlled and reproducible conditions.

Metabolic flux analysis (MFA) is one of the most efficient tools to analyze metabolic pathways, providing essential information on the biological system under study. The application of metabolic flux analysis using isotopically labeled substrates has been widely used to estimate the internal metabolic fluxes of a variety of organisms (Dauner and Sauer, 2001; Dauner et al., 2002; Kiefer et al., 2004; Jahn et al., 2013; Jeong et al., 2014; Kildegaard et al., 2016). In this approach, after the isotopic steady state is achieved, free metabolites can be analyzed or proteinogenic amino acids can be measured after biomass hydrolysis, allowing to infer about active metabolic pathways and carbon flow (Wittmann, 2007).

Studies using metabolic flux analysis and labeling experiments to assess *Salmonella* metabolism are very scarce. Xie et al. (2001) studied the impact of pyruvate carboxylase, if present in *S. typhimurium*, in oxaloacetate synthesis, cell growth, and metabolism, using MFA to quantify those effects. In another published study, ^{13}C-MFA was employed to analyze the carbon distribution in amino acids of the biomass of *S. typhimurium* growing inside mammalian cells (Gotz et al., 2010). Enos-Berlage and Downs (1999) studied the incorporation of glycine and formate into the pyrimidine moiety of thiamine pyrophosphate using ^{13}C-glycine and ^{13}C-formate.

Therefore, to broad the knowledge of *S. typhimurium* LT2 metabolism, and obtain experimental data under controlled conditions that can be used to improve the accuracy of metabolic model simulations, a ^{13}C MFA approach was applied to study the effect of growth rate on intracellular fluxes of *Salmonella typhimurium* LT2 growing in aerobic glucose-limited continuous cultures at two different dilution rates. The superimposition of the obtained flux distributions into the genome-scale metabolic model allowed evaluating the accuracy of the predictions made with this type of models.

In general, the improved knowledge of *S. typhimurium* metabolism will be essential not only to delineate strategies to fight *Salmonella* infections, but also for the development of metabolic engineering and cultivation strategies, to improve the production of biotechnological products using this host.

2. Materials and methods

Continuous cultures of *S. typhimurium* LT2 were conducted on glucose labeled with ^{13}C. The growth parameters, data on labeling of biomass protein hydrolysates and biomass composition were determined and used to generate metabolic flux distributions in central carbon pathways of *S. typhimurium* LT2. Subsequently, the experimental data were compared with simulations obtained using the existing genome-scale metabolic model, applying flux balance analysis (Fig. 1). The experimental procedures applied are detailed next.

2.1. S. typhimurium cultivation

Salmonella typhimurium LT2 was obtained from the *Salmonella* Genetic Stock Centre (University of Calgary, Canada). Inoculum preparation is detailed at Supplementary material 1.

Aerobic continuous cultivations were carried out in a 2 L bioreactor (Biostat B Plus, Sartorius, Germany), with a working volume of 800 mL, using M9 modified medium (composition available at Supplementary material 1).

An agitation speed of 750 rpm and an air flow rate of 1.25 SLPM, ensured that dissolved oxygen concentrations remained above 20% of saturation. The pH was controlled at 7.0 by automatic addition of NH_4OH (5%, v/v).

The medium was continuously fed to the bioreactor at a given dilution rate (D) (0.26 and 0.52 h^{-1}). The CO_2 concentration in the exhaust gas was analyzed using a carbon dioxide sensor (BCP-CO_2, BlueSens, Germany).

The steady state was inferred by tracking the optical density and the mole fraction of carbon dioxide in the exhaust gas, and it was considered to have been reached when these variables remained constant for at least two residence times. After the steady state was achieved, naturally labeled glucose in feed medium was replaced by 20% [U-^{13}C] glucose (99%, Omicron Bio) plus 80% (w/w) naturally labeled glucose, and the mixture was fed to the bioreactor for one residence time. Samples of cells were collected to analyze amino acids from cell protein. During the cultivation, samples were also collected to evaluate cellular growth, by-products production, and substrate consumption.

2.2. Dry cell weight and extracellular metabolite analysis

Cellular growth was followed by measuring the optical density of the culture at 600 nm ($OD_{600\,nm}$), using an ELISA microplate reader (TECAN Sunrise, Switzerland), and by determining the cellular dry weight (DW) (Smart et al., 2010).

The concentrations of glucose and extracellular metabolites (acetate, formate, lactate and succinate) were determined by HPLC (Jasco, Canada), using a Metacarb 87H column (300 × 7.8 mm, Varian, USA) and 5 mM sulfuric acid solution as the mobile phase (at a flow rate of 0.6 mL min^{-1}). The column temperature was 60 °C. Organic acids were detected using a UV detector at 210 nm (Jasco, Canada), while glucose was measured with a refractive index detector (Jasco, Canada). Acetate was also determined enzymatically with an acetic acid UV kit (R-Biopharm AG, Germany) according to the manufacturer's instruction.

2.3. ^{13}C labeling analysis

Gas Chromatography–Mass Spectrometry (GC-MS) of biomass protein hydrolysates was used for labeling analysis of proteinogenic amino acids of *S. typhimurium*. Briefly, 5 mL samples (in triplicate) were harvested from the culture, and the biomass protein was hydrolyzed. Then, samples were lyophilized for 24 h and the amino acids derivatized with methyl chloroformate (MCF) prior to GC-MS analysis (Villas-Bôas et al., 2003; Smart et al., 2010). GC-MS analysis is detailed at Supplementary material 1.

Mass isotopomer distributions (MIDs) of amino acid derivatives were calculated and corrected for the contribution of naturally abundant isotopes using IsoCor (Millard et al., 2012). An additional biomass correction was also applied, according to Nanchen et al. (2007), since the labeled substrate was fed to bioreactor only for one residence time and not all biomass became labeled with ^{13}C.

The fractional labeling was determined also according to Nanchen et al. (2007). The amino acids fragments with a fractional labeling with more than 20% of variation from the input substrate (20% of [U-^{13}C] glucose) were not considered for further analysis.

2.4. Metabolic flux calculations

A core metabolic network model of *S. typhimurium* was generated based on the published genome-scale metabolic model of *S. typhimurium* STM_v1.0 (Thiele et al., 2011), and includes the carbon atom transitions for each stoichiometric reaction. The generated model consisted of central carbon metabolic pathways, including glycolysis, pentose phosphate pathway, Entner-Doudoroff, tricarboxylic acid cycle, and anaplerotic reactions. Additionally, the pathways of amino acids

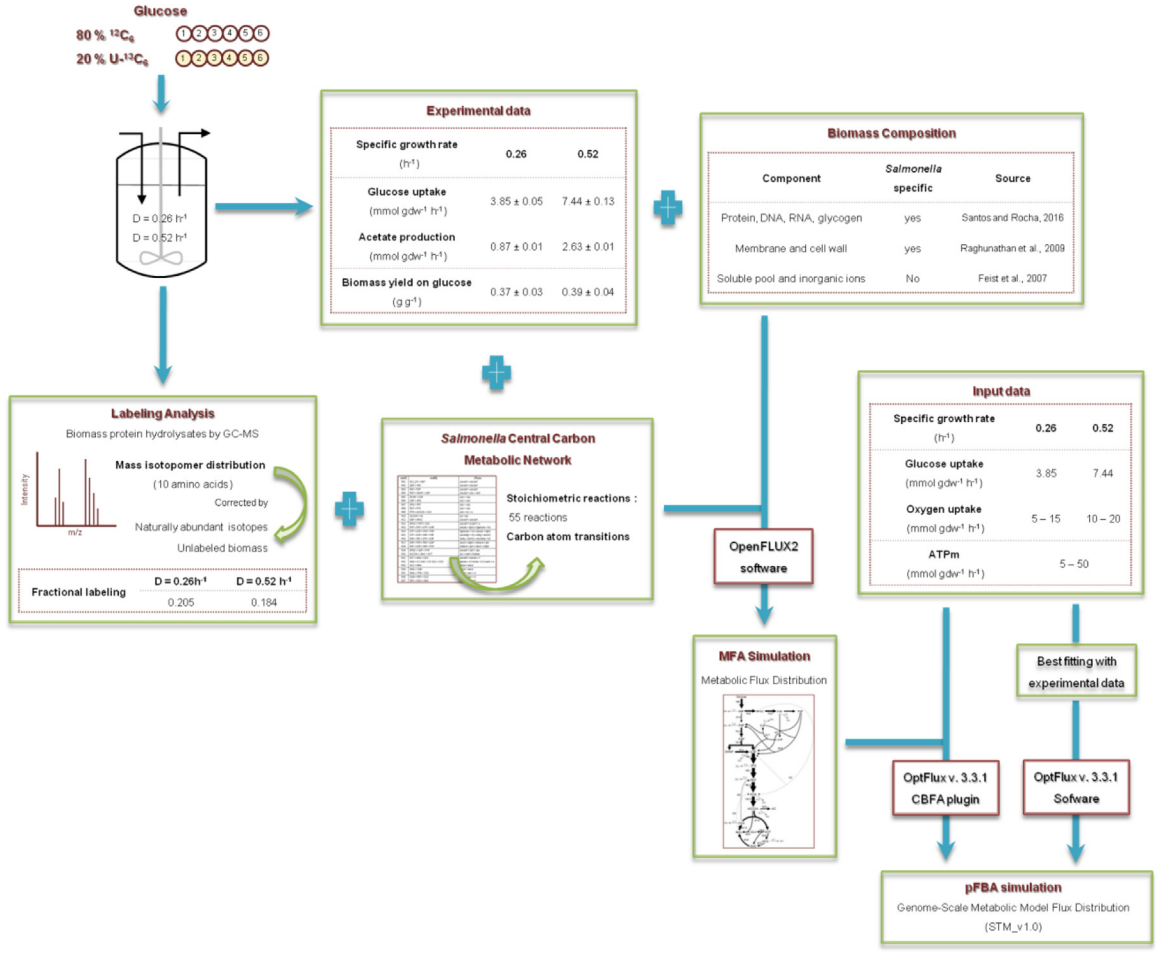

Fig. 1. Schematic representation of methods applied, data used to generate metabolic flux distributions and *in silico* methods and conditions. *S. typhimurium* LT2 was cultivated on 20% [U-^{13}C] glucose, under glucose-limited continuous culture conditions at D = 0.26 h^{-1} and D = 0.52 h^{-1}. Growth parameters, data on the analysis of labeling of biomass protein hydrolysates and biomass composition were used to generate metabolic flux distributions in central carbon pathways of *S. typhimurium* LT2. pFBA simulations were then performed using (or not) estimated fluxes and glucose uptake flux as input, varying the oxygen uptake and ATP maintenance (ATPm).

biosynthesis, acetate metabolism, and biomass reaction were also included, totalizing fifty-five stoichiometric reactions. Acetate was the only by-product incorporated in the model. The reversibility of reactions was established according to the genome-scale metabolic model (STM v1.0) (Thiele et al., 2011) and flux variability analysis. Therefore, pentose phosphate reactions were set as reversible. Successive reactions, without changes in atom transition, were lumped. The model was written according to the OpenFLUX instructions and examples (Quek et al., 2009; Quek and Nielsen, 2014; Shupletsov et al., 2014).

Metabolic precursor demands for biomass synthesis were calculated based on the *S. typhimurium* biomass composition previously described by Raghunathan et al. (2009) as well as from experimental data obtained by Santos and Rocha (2016, 2018) (detailed at Supplementary material 1).

Anabolic biomass demands, together with flux values of glucose uptake, acetate production, and biomass formation, were included as inputs to the model (Fig. 1). To obtain relative flux values, the fluxes included in the model were specified relative to 100 mmol of glucose uptake rate (Schatschneider et al., 2014).

To account for experimental measurement errors, mean and standard deviation of three technical replicates of MIDs, obtained for each dilution rate experiment, were calculated and used in the model. A total of 47 mass isotopomer fractions of amino acids from cell protein were used as input to determine the metabolic flux distributions.

Metabolic flux values were estimated using the MATLAB-based modeling software OpenFLUX2 (Shupletsov et al., 2014). Fluxes were computed 10 times, with 500 iterations, starting with random initial values. The statistical details are available at Supplementary material 1.

2.5. Genome-scale metabolic model simulations

The estimated intracellular metabolic fluxes were superimposed in the genome-scale STM_v1.0 metabolic model reconstructed for *S. typhimurium* by Thiele et al. (2011), which consists of 1270 genes, 2201 intracellular reactions, 345 exchange reactions, and 1119 metabolites. The biomass equation used in simulations was the same biomass equation used for metabolic flux calculations, as described in the metabolic calculation section (Section 2.4). Simulations were run with the OptFlux v. 3.3.1 open-source software platform (Rocha et al., 2010), using the Constraint-based Flux Analysis (CBFA) plugin (Carreira et al., 2014), which allowed including constraints associated with measured fluxes together with environmental conditions. The intracellular fluxes determined using OpenFLUX2 were used as measured fluxes with a margin error of 10% of the flux value. Glucose uptake flux was included as an environmental condition. The simulation method applied was the parsimonious flux-balance analysis (pFBA) with biomass maximization as the objective function (Lewis et al., 2010). Different oxygen uptake flux and ATPm (ATP maintenance requirement) coefficient values were tested in simulations. The oxygen uptake flux was varied from 5 to 15 mmol gDW^{-1} h^{-1} or from 10 to 20 mmol gDW^{-1} h^{-1}, for 0.26 h^{-1}

and 0.52 h^{-1} dilution rates, respectively. The ATPm coefficient ranged from 5 to 50 mmol gDW^{-1} h^{-1} for both dilution rates. The *in silico* results were compared with the experimental data obtained from the continuous experiments at the two studied dilution rates. The simulation conditions (ATPm and O_2) that resulted on the best fitting to experimental data were used to run pFBA simulation in Optflux (without the estimated measured fluxes) and intracellular fluxes estimated in *in silico* simulations were compared (Fig. 1).

3. Results and discussion

3.1. S. typhimurium continuous culture

In the present study, ^{13}C-MFA was applied to study *S. typhimurium* LT2 metabolism in aerobic glucose-limited chemostat cultivations under two different dilution rates (0.26 h^{-1} and 0.52 h^{-1}). The dilution rates were chosen based on previous results, which showed noticeable differences on the metabolic behavior of *S. typhimurium* growing at the mentioned dilution rates (Sargo et al., 2015). In our studies, 20% [U-^{13}C] glucose mixed with 80% naturally labeled glucose was used to explore *S. typhimurium* central carbon metabolism. In fluxomic studies using stable isotopic labeled substrates, the labeling should be selected according to the purpose of the study. Although the use of uniformly ^{13}C labeled glucose mixed with naturally labeled glucose has been debated recently (Crown et al., 2016) due to high confidence intervals in the estimations, it is an economic alternative to other substrates and has been recommended and successfully applied to study the metabolism of organisms, providing an overview of the most important pathways of the central carbon metabolism (Blank et al., 2005; Castillo et al., 2007; Chokkathukalam et al., 2014; Niu et al., 2013; Tao et al., 2012; Zamboni et al., 2009).

Growth parameters of *S. typhimurium* LT2 in glucose-limited continuous culture were determined (Fig. 1). The biomass yield obtained was similar in both dilution rates, and slightly higher than the one obtained for *S. typhimurium*, under the same conditions, by Sargo et al. (2015). Acetate was the unique by-product detected and was secreted in both dilution rates, with a production flux of 0.87 and 2.63 mmol gDW^{-1} h^{-1}, for D = 0.26 h^{-1} and D = 0.52 h^{-1}, respectively. Although the CO_2 concentration in the exhaust gas was analyzed and CO_2 production flux was determined (8.82 and 14.87 mmol gDW^{-1} h^{-1}, for D 0.26 h^{-1} and D = 0.52 h^{-1}, respectively) these data were not used for constraining metabolic flux distributions, since this flux may be higher than that determined, according to the carbon recovery obtained for both dilution rates (89% and 92%, for D = 0.26 h^{-1} and D = 0.52 h^{-1}, respectively) (Supplementary material 2).

Metabolic and isotopic steady state was achieved, as detailed at Supplementary material 3.

3.2. GC-MS-based labeling analysis

In ^{13}C labeling experiments, free metabolites can be analyzed or proteinogenic amino acids can be measured after biomass hydrolysis. The analysis of the amino acids of protein biomass provides extensive labeling information, being more abundant and less affected by errors (Wittmann, 2007). Labeling patterns of proteinogenic amino acids, obtained for instance by GC-MS, can be associated with their precursors, providing important information on central carbon metabolism (Nanchen et al., 2007).

In the present work, protein hydrolysates of biomass obtained in the continuous growth of *S. typhimurium* were analyzed by GC-MS. To obtain free amino acids, biomass protein underwent an acidic hydrolysis. During this process, cysteine and tryptophan are destroyed, and asparagine and glutamine are converted to aspartate and glutamate, respectively (Fountoulakis and Lahm, 1998). Thus, asparagine/aspartate and glutamine/glutamate are analyzed together. Moreover, arginine is not derivatized using the derivatization method applied (Smart et al., 2010).

From mass spectrometry (MS) raw data, the mass isotopomer distributions were calculated and corrected as described at item 2.4. To determine the fraction of unlabeled biomass, a first-order kinetics was applied, as proposed by Nanchen et al. (2007). Accordingly, since the ^{13}C glucose was fed to the bioreactor during one residence time, the fraction of unlabeled biomass was 0.368, for both dilution rates. It is known that using [U-^{13}C] glucose in labeling experiments, the fractional labeling (FL) of all amino acid fragments should be the same as the labeling content of the substrate (Nanchen et al., 2007), meaning that, in our experiments, the FL should be 20% for each amino acid fragment. As such, the actual experimental labeling was determined for each amino acid fragment to select the amino acid fragments that could be further used in calculations. A fractional labeling of 20% ± 4 was established as a criterion to accept the fragment for subsequent analysis. In general, mean FL values of 20.5% and 18.4% for 0.26 h^{-1} and 0.52 h^{-1}, respectively, were obtained and used as labeling percentage for the determination of metabolic flux distributions (Fig. 1). It is important to highlight that the theoretical FL (20%) was also used to run metabolic flux analysis, without significant differences in the estimated intracellular fluxes.

Based on the relative error of mass isotopomer distributions, 10 amino acids derivatives (alanine, aspartate, glutamate, glycine, lysine, proline, serine, threonine, tyrosine, and valine) were selected to use as inputs for the determination of metabolic flux distributions (Supplementary material 4).

3.3. S. typhimurium core metabolic network and metabolic flux analysis

The generated *S. typhimurium* LT2 core model consisted of 55 reactions, 45 intracellular metabolites and 3 extracellular metabolites (Supplementary material 5).

In order to determine the metabolite precursor demands for biomass, the contribution of each biomass component was determined and adjusted to account for all components. After that, the biomass precursor demands were calculated and are presented at Supplementary material 6.

To evaluate the data consistency, experimental mass isotopomer fractions were plotted versus simulated mass isotopomer fractions obtained in MFA simulations for all amino acids, for each dilution rate (Supplementary material 7). This analysis showed the agreement between experimental and simulated data, also corroborated by the mean deviation between experimental and simulated data (29%, for both dilution rates). The differences between experimental and estimated MIDs can be explained, in part, by the high experimental standard deviations observed for some mass isotopomers (Supplementary material 4).

3.4. Impact of growth rate on central carbon metabolic flux distributions

The cell physiology of an organism is highly influenced by the growth rate, with the cell adapting its metabolism according to the availability of carbon and energy, as demonstrated for *E. coli* (Kayser et al., 2008; Valgepea et al., 2011). The best estimation of *in vivo* intracellular flux distributions of *S. typhimurium* LT2 growing under glucose-limited continuous culture conditions at the studied dilution rates are showed in Fig. 2. Three possible pathways for glucose catabolism are present in *S. typhimurium*, namely Glycolysis, the Pentose Phosphate and the Entner-Doudoroff (ED) pathways. Glucose catabolism via glycolysis was described (Driessen et al., 1987) and seems to be the most important route that functions in *S. typhimurium* during infection of macrophages and mice (Bowden et al., 2009). The ED pathway was also reported to be important in *Salmonella* within macrophages for the utilization of some carbon sources, such as gluconate (Diacovich et al., 2017; Eriksson et al., 2003).

The flux distributions obtained in the present work suggested that

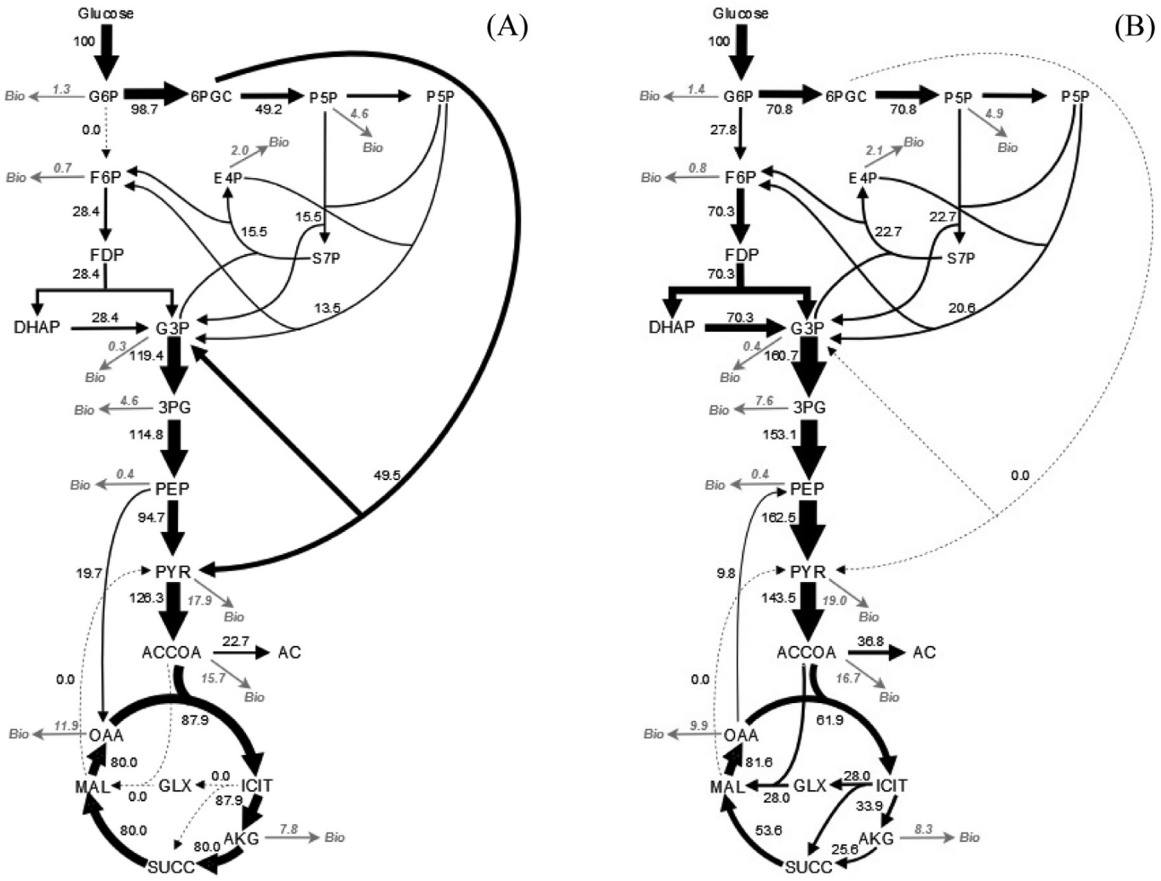

Fig. 2. *In vivo* metabolic flux distributions in the central carbon pathways of *S. typhimurium* LT2 growing under glucose-limited continuous culture conditions at D = 0.26 h^{-1}(A) and D = 0.52 h^{-1}(B). Fluxes relative to 100 mmol of glucose uptake rate. Arrows thickness is proportional to flux. Fluxes to biomass are indicated in gray. Abbreviations: 3PG – 3-Phospho-D-glycerate, 6PGC – 6-Phospho-D-gluconate, AC – Acetate, ACCOA – Acetyl-CoA, AKG – 2-Oxoglutarate, DHAP – Dihydroxyacetone-phosphate, E4P – D-Erythrose-4-phosphate, F6P – D-Fructose-6-phosphate, FDP – D-Fructose-1–6-bisphosphate, G3P – Glyceraldehyde-3-phosphate, G6P – D-Glucose-6-phosphate, GLC – D-Glucose, GLX – Glyoxylate, ICIT – Isocitrate, MAL – L-Malate, OAA – Oxaloacetate, P5P – Pentose-5-phosphate, PEP – Phosphoenolpyruvate, PYR – Pyruvate, S7P – Sedoheptulose-7-phosphate, SUCC – Succinate.

glucose is mostly catabolized via pentose phosphate at the studied growth conditions. At D = 0.52 h^{-1}, 70.8% of glucose flux was catabolized by the pentose phosphate pathway and a small percentage by glycolysis (27.8%), while for D = 0.26 h^{-1}, the pentose phosphate is utilized together with ED, with 49.2% of glucose being catabolized by the last.

Simulation results suggested a low ED pathway flux at 0.52 h^{-1}. Even though there is no available information about the use of ED pathway by *Salmonella* during growth with glucose, it is proven that some organisms can use the ED pathway to catabolize glucose, such as *Z. mobilis, P. fluorescens, S. meliloti, A. tumefaciens, P. versutus, R. sphaeroides, X. campestris* (Fuhrer et al., 2005; Schatschneider et al., 2014). According to Conway (1992), this pathway is more primitive than glycolysis.

Flamholza and collaborators (2013) conducted a study to exploit the use of glycolytic and ED pathways in prokaryotes. Although the main difference between ED and glycolysis is the ATP production, being produced one ATP in ED and two in glycolysis, they hypothesized that the enzymatic synthesis cost also plays a key role in the choice of the pathway used for glucose catabolism. The use of the ED pathway results in a lower protein synthesis cost to catabolize the same amount of glucose than glycolysis (Flamholza et al., 2013). They also suggested that, for organisms that possess another form of ATP production, which is the case of *S. typhimurium*, the ED pathway would be preferentially used, considering that protein synthesis limits growth (Flamholza et al., 2013). Despite that, the influence of growth rate on the catabolic pathway used is still not clarified. Taking together our data and the hypothesis exposed by Flamholza et al. (2013), we can hypothesize that at a lower growth rate (D = 0.26 h^{-1}) and under balanced growth conditions, there would be no ATP limitation but rather protein synthesis would be the limiting step for growth. On the other hand, at D = 0.52 h^{-1}, the ATP produced in ED pathway seems insufficient, and the cell utilizes the glycolysis to compensate the energetic needs. The modulation of the utilization of these pathways by the growth rate is a hypothesis that needs yet to be proven, for example, by investigating protein expression under these conditions. The use of positional labeling of glucose could also be applied to prove the arising hypothesis. For instance, [1,2- ^{13}C] glucose or [1–^{13}C] glucose could be applied to clarify the activation of ED pathway, as reported by other authors (Hollinshead et al., 2015; Schatschneider et al., 2014). In addition, data on dilution rates lower than D = 0.26 h^{-1} would contribute to clarify these assumptions.

The excess flux in the pentose phosphate pathway returned to fructose-6-phosphate and continued to the glycolytic pathway, more intensely at D = 0.52 h^{-1}. The fluxes through the tricarboxylic acid cycle decreased with increasing growth rates. This relative increase of pentose phosphate fluxes and the decrease of TCA cycle fluxes with increasing dilution rates were also observed by Kayser et al. (2005) in *E. coli* glucose-limited chemostat cultures, especially at growth rates higher than 0.3 h^{-1}. This limitation in the TCA cycle may also be associated with a relatively lower respiratory rate at higher dilution rates, which may contribute to an increased limitation in the availability of ATP, favouring the utilization of Glycolysis in replacement of the ED pathway, as described above.

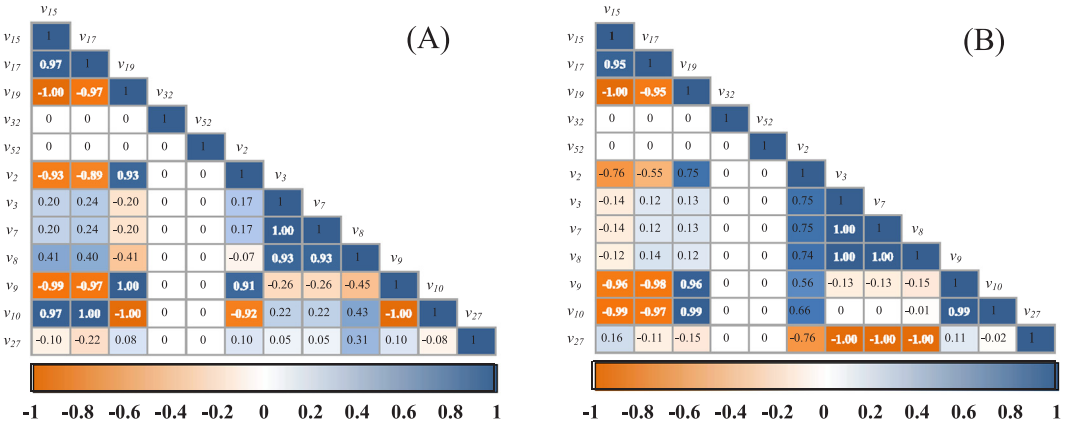

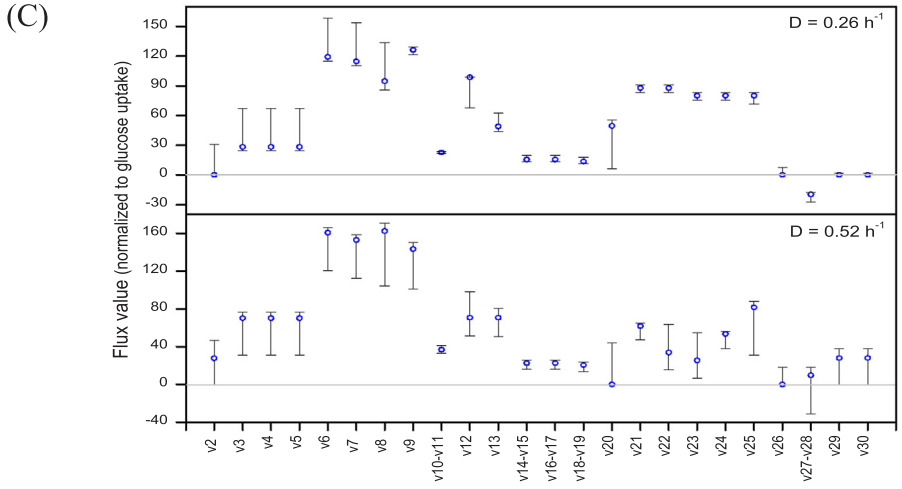

(D)

Flux (*v*)	Reaction	Metabolic pathway
2	G6P = F6P	Glycolysis
3	F6P = FDP	Glycolysis
4	FDP = DHAP + G3P	Glycolysis
5	DHAP = G3P	Glycolysis
6	G3P = 3PG	Glycolysis
7	3PG = PEP	Glycolysis
8	PEP = PYR	Glycolysis
9	PYR = ACCOA + CO2	Glycolysis
10-11	ACCOA = AC / AC = ACCOA	Acetate metabolism
12	G6P = 6PGC	Pentose phosphate / Entner-Doudoroff
13	6PGC = P5P + CO2	Pentose phosphate
14-15	P5P + P5P = S7P + G3P / S7P + G3P = P5P + P5P	Pentose phosphate
16-17	S7P + G3P = E4P + F6P / E4P + F6P = S7P + G3P	Pentose phosphate
18-19	E4P + P5P = F6P + G3P / F6P + G3P = E4P + P5P	Pentose phosphate
20	6PGC = G3P + PYR	Entner-Doudoroff
21	ACCOA + OAA = ICIT	TCA Cycle
22	ICIT = AKG + CO2	TCA Cycle
23	AKG = SUCC + CO2	TCA Cycle
24	SUCC = MAL	TCA Cycle
25	MAL = OAA	TCA Cycle
26	MAL = PYR + CO2	Anaplerotic
27-28	OAA = PEP + CO2 / PEP + CO2 = OAA	Anaplerotic
29	ICIT = GLX + SUCC	Anaplerotic
30	GLX + ACCOA = MAL	Anaplerotic
32	AC = AC_EX	Extracellular
52	Biomass	Biomass Production

Fig. 3. Correlation matrixes between free fluxes (A and B). Correlation values between free fluxes are represented as a gradient of colors from orange (−1) to dark blue (+1). Correlation values that represent a very high correlation are highlighted in white writing. (A): D = 0.26 h^{-1} and (B): D = 0.52 h^{-1}. Optimum values (circles) and associated 95% of confidence interval using a non-linear approach for fluxes of reactions at D = 0.26 h^{-1} and D = 0.52 h^{-1} (C). List of reactions and associated metabolic pathways (D). Abbreviations in Fig. 2.

The increase of the relative flux going to the pentose phosphate pathway at higher growth rates points to the necessity of producing reducing equivalents in the form of NADPH for biosynthesis, as well as cell precursors, evidencing the anabolic function of this pathway. This result is, however, in contrast with the results obtained by Haverkorn van Rijsewijk et al. (2011) that showed that the relative flux into the PP pathway is not affected by the growth rate in *E. coli* growing on glucose. To further elucidate the flux ratio between the pentose phosphate pathway and glycolysis in *S. typhimurium*, future analysis using [1–^{13}C] glucose could be used as the 1st ^{13}C labeled carbon is released as CO_2 in the oxidative PP pathway, whereas it is conserved in the glycolysis (Toya et al., 2010).

Acetate was produced in both studied dilution rates. An increase of acetate production rate was observed with increasing growth rates, showing the overflow effect, also reported in our previous work on *S. typhimurium* (Sargo et al., 2015). Although the overflow metabolism is an intricate phenomenon that is regulated at different cellular levels, it is recognized that the growth rate acts as a modulator of the overflow metabolism (for review see Bernal et al., 2016). An increase in this phenomenon at higher growth rates is also consistent with the lower relative activity observed for the TCA cycle.

In *E. coli,* acetate overflow and assimilation patterns vary with the strain. For instance, *E. coli* K-12 strain can only assimilate acetate after the exhaustion of glucose in the culture medium, while *E. coli* BL21 accumulates less acetate due to the lower catabolite repression, being possible a simultaneous assimilation of acetate and glucose, using the glyoxylate cycle (Bernal et al., 2016; Phue et al., 2005; Waegeman et al., 2012). The assimilation of acetate concomitantly with glucose consumption has not been described for *S. typhimurium*. In our results, the high levels of acetate accumulation at D = 0.52 h^{-1} are coherent with no or a low acetate assimilation (Sargo et al., 2015). On the other hand, the activation of the glyoxylate shunt is only visible at D = 0.52 h^{-1}.

The glyoxylate shunt is usually inactive under growth with glucose and is commonly used for growth solely on acetate and other 2-carbon substrates (Bernal et al., 2016). In *Salmonella,* the glyoxylate pathway was characterized by Wilson and Malloy (1987) and is known to be transcriptionally regulated. Isocitrate lyase (*aceA*) and malate synthase (*aceB*) are two enzymes involved in this pathway and are induced during growth with acetate. *aceA* and *aceB* genes are at the same operon and have repressors encoded by *iclR* and *fadR* genes (Wilson and Malloy, 1987). In *E. coli,* the knock-out of *iclR* (isocitrate lyase regulator) increases the expression of *aceA* and *aceB*, with a consequent activation of the glyoxylate pathway, as shown in *E. coli* BL21 (Liu et al., 2017). The glyoxyate pathway can also be regulated by *icd,* which encodes for the isocitrate dehydrogenase, modulating the metabolic flux between the TCA cycle and the glyoxylate shunt. This node seems to be regulated by the growth rate, since in glucose-limiting conditions it was observed that the activity of this enzyme decreased with the increase of the growth rate (Chao et al., 1997).

On the other hand, Fischer and Sauer (2003) described a cycle called phosphoenolpyruvate (PEP)-glyoxylate cycle in *Escherichia coli*. In the described route, PEP carboxykinase and glyoxylate shunt enzymes are active at the same time. Parallel operation of TCA cycle and PEP-glyoxylate cycle in *Escherichia coli* growing in continuous culture at low dilution rates (0.12 h^{-1}) was observed (Fischer and Sauer, 2003). In addition, Haverkorn van Rijsewijk et al. (2011) studied the regulation associated with the distribution of metabolic fluxes in *E. coli* growing aerobically with glucose and galactose and proved that in glucose-limited growth conditions, the increase of dilution rate diminished the percentage of relative flux through PEP-glyoxylate cycle. They also pointed to possible transcriptional regulation at the acetyl-CoA branch point, distributing the flux between acetate overflow and the TCA cycle (Haverkorn van Rijsewijk et al., 2011).

At dilution rate of 0.52 h^{-1} the anaplerotic reaction (OAA = PEP + CO_2), catalyzed by PEP carboxykinase is active (9.8%) together with the glyoxylate cycle, as well as TCA cycle, suggesting the presence of (PEP)-glyoxylate cycle in *Salmonella typhimurium* LT2 (Fig. 2). However, there is a remarkable difference in the growth rate in which this cycle was observed in the published works (Haverkorn van Rijsewijk et al., 2011; Fischer and Sauer, 2003) and the one verified in the present work.

In summary, the fact that the glyoxylate cycle is activated at high dilution rates seems to be in opposite directions as what has been described for *E. coli* regarding the PEP-glyoxylate cycle. The regulatory patterns of acetate consumption and glyoxylate cycle remain to be described for *Salmonella*, as well as the role of the isocitrate dehydrogenase in this organism. According to Maeda et al. (2016), the mixture of non-labeled, [1–^{13}C] and [U-^{13}C] glucose at ratios of 4:1:5 could be applied to estimate the metabolic fluxes through glyoxylate pathway with higher precision.

3.4.1. Statistical evaluation of estimated flux distributions

A correlation matrix of free fluxes was generated to study the relationship between fluxes (Fig. 3A and B). In general, pentose phosphate fluxes and acetate biosynthesis flux were shown to be particularly correlated with the other free fluxes. Due to network structure, it was expected that some fluxes were highly correlated, which was verified for the pentose phosphate fluxes (v_{15}, v_{17}, and v_{19}). Another example was the correlation between v_2 (G6P = F6P) and pentose phosphate fluxes (v_{15}, v_{17}, and v_{19}). Furthermore, some unexpected correlations arose, such as the high correlation between v_{10} (acetate production) and pentose phosphate fluxes. Moreover, it is important to stress that there were noticeable differences in correlations between fluxes at the studied dilution rates. For instance, acetate production flux (v_{10}) showed an opposite correlation at the different studied dilution rates, presenting a positive correlation with v_{15} and v_{17} (pentose phosphate fluxes) and a negative correlation with v_{19} (also a pentose phosphate flux) for D = 0.26 h^{-1} and the opposite correlations for D = 0.52 h^{-1}. These observed differences in correlations emphasize the different metabolic behaviors observed at the different growth rates.

Correlations between biomass formation (v_{52}) and other free fluxes were not observed, which was not expected since glycolysis and pentose phosphate pathway contributes with precursors to biomass formation.

In the determination of metabolic flux distributions, it is important to study the uncertainty and variability of the obtained results. It must be stressed that the estimated fluxes with wider confidence intervals must be analyzed carefully to avoid misleading interpretations. Thus, the sensitivity of estimated metabolic fluxes was determined using a non-linear approach with 95% of confidence, implemented in OpenFLUX2 (Shupletsov et al., 2014) (Fig. 3C). In general, the probability distributions showed that the estimated intracellular fluxes for D = 0.26 h^{-1} present higher sensitivity than the ones estimated for D = 0.52 h^{-1}. Glycolysis reaction fluxes v_2-v_7 showed wide intervals, while v_{14} - v_{19} pentose phosphate reactions presented narrow confidence intervals, for both growth rates. TCA cycle reaction fluxes v_{21}-v_{24} presented higher flux values with a narrow confidence interval at D = 0.26 h^{-1} comparing with D = 0.52 h^{-1}. The confidence limits determined for Entner-Doudoroff reaction flux (v_{20}) at D = 0.26 h^{-1} showed that this reaction will have a flux between (6.5 and 55.7), with 95% of confidence. Although the determined interval is large, it is different from that obtained for D = 0.52 h^{-1} (0–44.3), indicating a greater probability that this pathway is being activated at the lowest growth rate. For glyoxylate cycle reactions, a wide interval was observed for D = 0.52 h^{-1} with an optimum flux value of 28, while the glyoxylate cycle will be inactive or with very low flux (1.65), with 95% of confidence, at D = 0.26 h^{-1}.

It is known that the determination of metabolic fluxes is affected by a variety of errors. Besides the choice of the isotopic tracer, analytical labeling analysis procedures and the structure of metabolic network are factors that contribute to the uncertainties of the flux estimation (Crown et al., 2016; Leighty and Antoniewicz, 2012; Mairinger et al.,

2018). Nevertheless, it is important to highlight that the present work was conducted with the aim of explore the *S. typhimurium* metabolism, raising hypothesis to be further explored.

3.5. *In vivo vs. in silico S. typhimurium metabolic fluxes*

In order to compare the experimental data with *in silico* simulation results and investigate the suitability of the genome-scale metabolic model to describe *S. typhimurium* metabolism, simulations were performed using pFBA.

Using the extracellular flux of glucose as constraint and considering unlimited oxygen uptake, the genome-scale metabolic model predicts a specific growth rate of 0.39 h^{-1} for the lower dilution rate and 0.79 h^{-1} for the higher one, which are higher than the ones obtained *in vivo*. This discrepancy can be justified by the presence of acetate *in vivo*, which is not predicted by the model under full aerobic conditions. In fact, using stoichiometric models it is only possible to mimic the overflow metabolism by constraining artificially the oxygen uptake rate. If the experimentally determined fluxes (extracellular flux of glucose as well as intracellular fluxes $v_2 - v_{30}$ indicated in Fig. 3D) are used as constraints and also considering unlimited oxygen uptake, the genome-scale model predicts a specific growth rates more closely to the ones obtained *in vivo* (0.30 h^{-1} for the lower dilution rate and 0.58 h^{-1} for the higher one). Besides that, ATP coefficient associated with non-growth maintenance (ATPm), although kept fixed in metabolic models, is known to vary with the growth rate of an organism (Russel and Cook, 1995).

Given these results, we have performed additional pFBA simulations to map the influence of oxygen uptake and the ATPm coefficient in model outputs. Simulations using the Optflux - CBFA plugin were run with the same estimated intracellular fluxes previously selected as constraints and glucose uptake flux as environmental condition. The results of simulations (Fig. 4) show that the *in silico* biomass formation rate varies with ATPm coefficient and oxygen uptake rate. If the oxygen uptake increases, it is necessary to increase the ATPm coefficient to fit the *in silico* to experimental specific growth rate (Fig. 4 – A and C). The prediction of acetate production is also affected by the oxygen uptake rate and ATPm coefficient. The production of this metabolite is only predicted at ATPm coefficients higher than 15 mmol ATP gDW^{-1} h^{-1} and oxygen uptake rates higher than 10 mmol O_2 gDW^{-1} $h^{-1}$for D = 0.26 h^{-1}; and ATPm coefficients higher than 30 and oxygen uptake rates higher than 15 for D = 0.52 h^{-1} (Fig. 4 – B and D). Besides acetate, the formation of other by-products, such as ethanol and formate, was predicted by the simulations, but not observed experimentally. For D = 0.52 h^{-1}, ethanol production was predicted for almost every simulation conditions, whereas, at D = 0.26 h^{-1}, ethanol formation was predicted especially for lower values of oxygen uptake and ATPm coefficients (below 12 mmol gDW^{-1} h^{-1} and 15 mmol gDW^{-1} h^{-1}, respectively). In fact, ethanol is predicted to be produced, instead of acetate, for ATPm coefficients lower than 30 and 15, for D = 0.26 h^{-1} and D = 0.52 h^{-1}, respectively. For D = 0.52 h^{-1} all simulation conditions predicted the production of another by-product than acetate (Supplementary material 8). Ethanol and formate are known to be by-products formed under anaerobiosis (Sargo et al., 2015). Thus, at the condition of aerobiosis used in the present work the formation of these metabolites would not be expected.

It is known that, for *Salmonella* and *E. coli*, acetate production is beneficial in energetic terms when compared with the production of other by-products such as ethanol (one extra ATP molecule formed when acetate is produced) (Wolfe, 2005). Thus, under aerobic conditions and given the possibility of using other means of re-oxidizing the reduced NAD cofactor, these organisms excrete acetate under overflow conditions. The fact that the genome-scale model, constrained by the measured fluxes, predicts that acetate only needs to be excreted when ATPm is high reflects this phenomenon. With a lower ATPm the cells seem to have no energetic limitations and thus could excrete the overflow carbon in the form of ethanol, without gaining the extra ATP. With a higher ATPm, cells pass into an energy-limiting condition and acetate is the only product that can be excreted. The differences observed between both dilution rates are difficult to discuss, as the impact of the oxygen uptake is higher at a higher dilution rate. Clearly, at lower oxygen uptake rates (under oxygen limitation), ethanol needs to be excreted as a way to recycle the reduced cofactors.

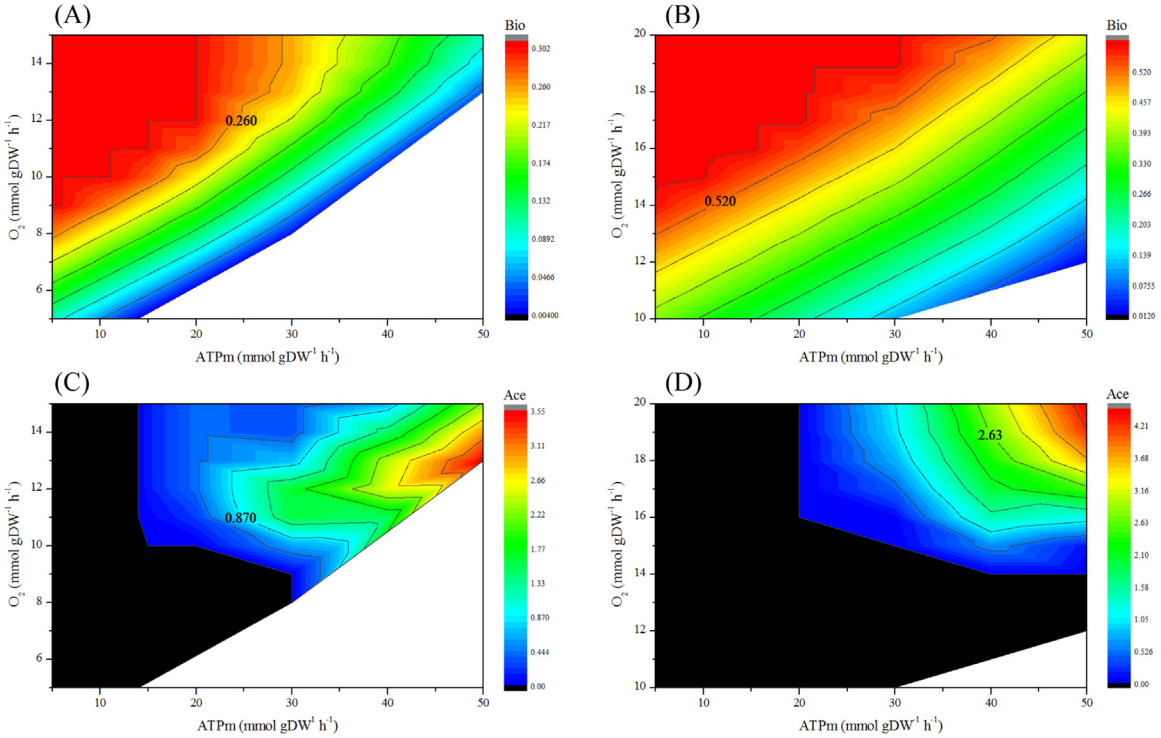

Fig. 4. Contour maps of CBFA simulations using estimated fluxes as measured fluxes and glucose uptake flux as input. Variation of biomass (A and C) and acetate (B and D) production fluxes with oxygen uptake flux and ATPm flux. Experimental values marked in graphs. (A) and (B): D = 0.26 h^{-1} and (C) and (D): D = 0.52 h^{-1}.

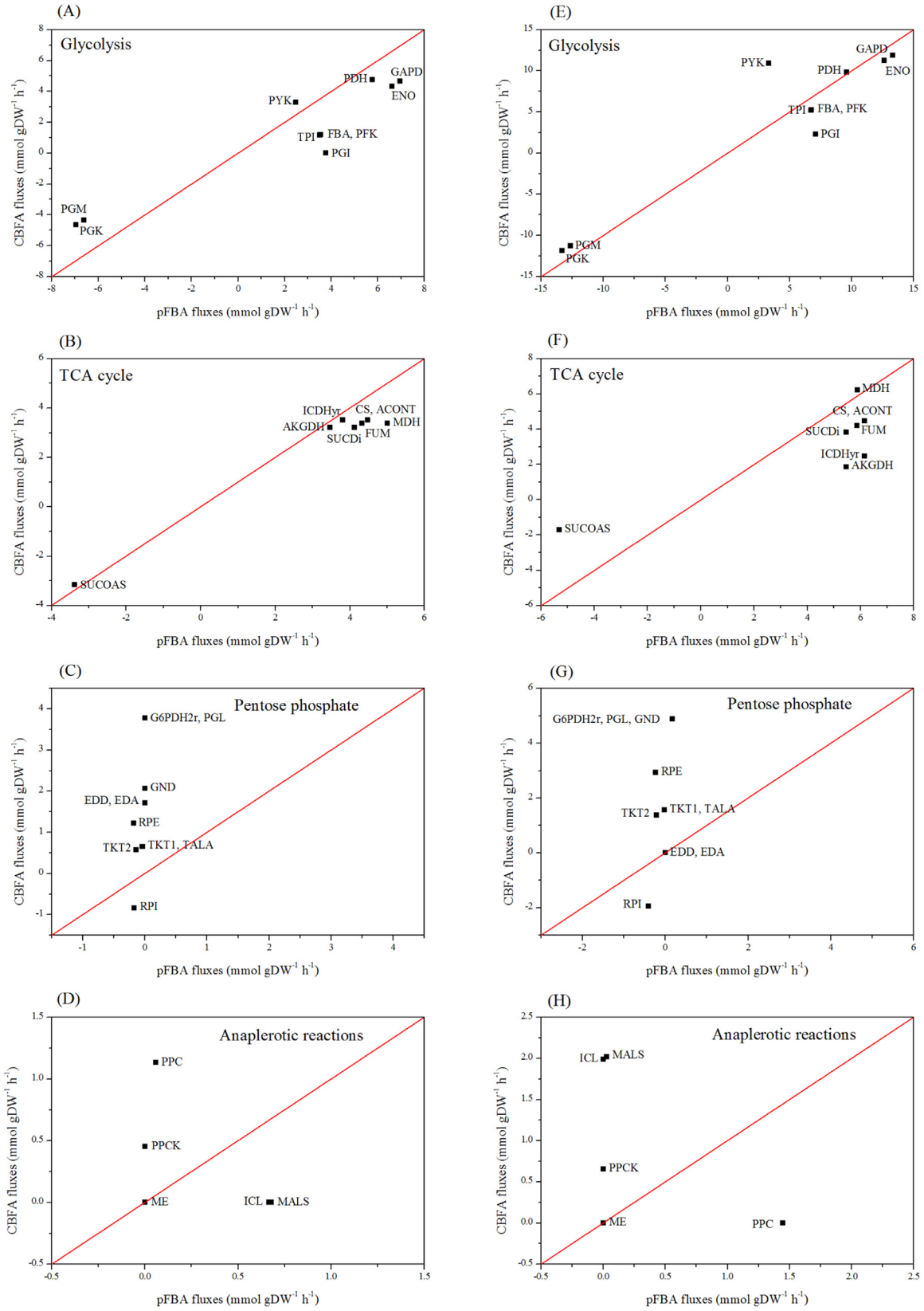

(caption on next page)

In the *S. typhimurium* genome-scale metabolic model (STM_v1.0) reconstructed by Thiele et al. (2011), the default value for ATPm is 8.39 mmol gDW^{-1} h^{-1}, which was determined for *E. coli* (Feist et al., 2007). Nevertheless, in general, and assuming that ATPm levels as high as 20 mmol gDW^{-1} h^{-1} are not physiologically possible, we can conclude that *Salmonella* cells seem to be in an ATP non-limiting condition for both dilution rates. This hypothesis was already raised above when concerning the lower dilution rate for the discussion on the utilization

Fig. 5. Comparison of flux values of intracellular reactions obtained in CBFA simulation with the ones predicted by pFBA simulation. The simulations were run using the experimental flux of glucose with the best oxygen uptake flux and ATPm flux for each dilution rate. (A) to (D): D = 0.26 h^{-1}, oxygen uptake flux = 13 mmol gDW^{-1} h^{-1}, ATPm flux = 30 mmol gDW^{-1} h^{-1} and (E) to (H): D = 0.52 h^{-1}, oxygen uptake flux = 20 mmol gDW^{-1} h^{-1}, ATPm flux = 40 mmol gDW^{-1} h^{-1}. The reactions are grouped by metabolic pathways: glycolysis, TCA cycle, pentose phosphate pathway (including Entner-Doudoroff) and anaplerotic reactions. Abbreviations: Glycolysis: ENO – enolase, FBA - fructose bisphosphate aldolase, GAPD - glyceraldehyde 3 phosphate dehydrogenase, PDH - pyruvate dehydrogenase, PFK – phosphofructokinase, PGI - glucose 6 phosphate isomerase, PGK - phosphoglycerate kinase, PGM - phosphoglyceratemutase, PYK - pyruvate kinase, TPI - triose phosphate isomerase; TCA cycle: ACONT – Aconitase half-reaction A Citrate hydro-lyase and Aconitase half-reaction B Isocitrate hydro-lyase, AKGDH - 2 Oxoglutarate dehydrogenase, CS - citrate synthase, FUM – fumarase, ICDHyr - isocitrate dehydrogenase NADP, MDH - malate dehydrogenase, SUCDi - succinate dehydrogenase irreversible, SUCOAS - succinyl-CoA synthetase ADP-forming; Pentose phosphate: EDA - 2 dihydro 3 deoxy phosphogluconate aldolase, EDD - 6 phosphogluconate dehydratase, G6PDH2r - glucose 6 phosphate dehydrogenase, GND - phosphogluconate dehydrogenase, PGL - 6 phosphogluconolactonase, RPE - ribulose 5 phosphate 3 epimerase, RPI - ribose 5 phosphate isomerase, TALA – transaldolase, TKT1,2 – transketolase; Anaplerotic reactions: ICL – isocitrate lyase, MALS – malate synthase, ME - malic enzyme NAD and malic enzyme NADP, PPC - phosphoenolpyruvate carboxylase, PPCK – phosphoenolpyruvate carboxykinase.

of the ED pathway. The fact that ethanol is not produced *in vivo* instead of acetate, if this hypothesis is true, is probably related with regulatory constraints.

As a way to evaluate the predictions made solely with the genome-scale metabolic model, we have compared the results of pFBA simulation without constraining the measured fluxes with the CBFA simulation where all the measured fluxed were used as constraints (Fig. 5). Generally, pFBA simulations presented higher fluxes than CBFA for glycolysis and the TCA cycle reactions, for both dilution rates (Fig. 5A, B, E, F). Pentose phosphate reactions presented a very low flux in pFBA simulation compared with CBFA simulation (Fig. 5C and G), showing that the genome-scale metabolic model does not adequately describe the experimental fluxes through this pathway, as was already reported for other organisms (Pereira et al., 2016). pFBA simulation also failed to predict flux in the Entner–Doudoroff pathway at D = 0.26 h^{-1}. The flux values in anaplerotic reactions were also very different in pFBA simulation and CBFA (Fig. 5D and H), with glyoxylate cycle activated in pFBA simulation at D = 0.26 h^{-1} instead of at D = 0.52 h^{-1} (obtained for CBFA).

4. Conclusions

This work represents, to the best of our knowledge, the first study describing the carbon flow in the central carbon metabolic network of *S. typhimurium* growing at glucose-limited chemostat cultures under two different dilution rates (0.26 h^{-1} and 0.52 h^{-1}).

Several conclusions can be drawn regarding the utilization of pathways for glucose catabolism. Differences in flux distributions in central carbon reactions between growth rates were observed. Besides glycolysis, pentose phosphate pathway is utilized to a higher extent. The results suggested that the Entner-Doudoroff pathway and the glyoxylate shunt were also activated at D = 0.26 h^{-1} and D = 0.52 h^{-1}, respectively. Such hypotheses could be elucidated by: (1) the inclusion of $^{13}CO_2$ measures to extend the metabolic network model and improve its accuracy (Leighty and Antoniewicz, 2012); (2) employing optimization methods such as D-optimality criterion in order to select appropriates isotopic tracers for a precise estimation of fluxes depending on the interested pathway (Crown and Antoniewicz, 2012); and (3) performing multiple parallel labeling experiments to generate complementary labeling information that can improve the resolution of fluxes and also allow the *S. typhimurium* model validation (Leighty and Antoniewicz, 2012).

Overall, the obtained results point, on one hand, to a flexible metabolism in *Salmonella typhimurium*, with the possibility of the use of different pathways with similar functions but, on the other hand, to the need of performing further experiments to understand the regulation of the glyoxylate shunt and acetate metabolism, which seem to behave differently when compared with what has been observed for *E. coli*.

In silico studies were performed to infer about genome-scale metabolic model precision. In general, pFBA simulation using the CBFA OptFlux plugin with estimated intracellular fluxes as constraints showed a better fitting with extracellular fluxes, thus improving the accuracy of metabolic model simulations. Regarding intracellular fluxes, it is noticeable that some pathways, such as the pentose phosphate and anaplerotic reactions are not well described by pFBA using the genome-scale metabolic model (STM_v1.0), a limitation that seems to be common to many genome-scale models.

We also raise here the hypothesis of, at least at the lower dilution rate, the cells not being energy-limited, justifying the utilization of the ED pathway and the results obtained analyzing the flux space constrained by the measured fluxes. Although, this hypothesis still needs to be proven.

Besides the contribution to broad the knowledge of *S. typhimurium* metabolism, the data presented here might be useful to modulate and optimize the growth of this organism with important medical and biotechnological applications.

Acknowledgments

This work was in part financed by the Coordenação de Aperfeiçoamento de Pessoal de Nível Superior, Brazil (CAPES) – Finance code 001. The authors also acknowledge the support of CNPq (Conselho Nacional de Desenvolvimento Científico e Tecnológico, Brazil); International cooperation project CAPES-FCT (Coordenacão de Aperfeiçoamento de Pessoal de Nível Superior/Brazil - Fundação para a Ciência e Tecnologia/Portugal - Process 315/11); CAPES, Brazil (Atração de Jovens Talentos - Process 064922/2014-01); Fundação para a Ciência e Tecnologia, Portugal (strategic funding of UID/BIO/04469 unit) and COMPETE 2020, Portugal (POCI-01-0145-FEDER-006684), in addition to the BioTecNorte operation (NORTE-01-0145-FEDER-000004) funded by European Regional Development Fund under the scope of Norte2020 - Programa Operacional Regional do Norte.

Appendix A. Supporting information

Supplementary data associated with this article can be found in the online version at doi:10.1016/j.ymben.2018.11.011

References

Abuon, M., Suthers, P.F., Jones, G.I., Carter, B.R., Saunders, M.P., Maranas, C.D., Woodward, M.J., Anjum, M.F., 2009. Genome scale reconstruction of a *Salmonella* metabolic model: comparison of similarity and differences with a commensal *Escherichia coli* strain. J. Biol. Chem. 284, 29480–29488.

Bernal, V., Castaño-Cerezo, S., Cánovas, M., 2016. Acetate metabolism regulation in *Escherichia coli*: carbon overflow, pathogenicity, and beyond. Appl. Microbiol. Biotechnol. 100, 8985–9001.

Blank, L.M., Kuepfer, L., Sauer, U., 2005. Large-scale ^{13}C-flux analysis reveals mechanistic principles of metabolic network robustness to null mutations in yeast. Genome Biol. 6, R49.

Bolhassani, A., Zahedifard, F., 2012. Therapeutic live vaccines as a potential anticancer strategy. Int. J. Cancer 131 (8), 1733–1743.

Bowden, S.D., Rowley, G., Hinton, J.C., Thompson, A., 2009. Glucose and glycolysis are required for the successful infection of macrophages and mice in *Salmonella enteric* serovar Typhimurium. Infect. Immun. 77, 3117–3126.

Braga, C.J., Massis, L.M., Sbrogio-Almeida, M.E., Alencar, B.C., Bargieri, D.Y., Boscardin, S.B., Rodrigues, M.M., Ferreira, L.C., 2010. CD8+ T cell adjuvant effects of *Salmonella* FliCd flagellin in live vaccine vectors or as purified protein. Vaccine 28, 1373–1382.

Carreira, R., Evangelista, P., Maia, P., Vilaça, P., Pont, M., Tomb, J.F., Rocha, I., Rocha, M., 2014. CBFA: phenotype prediction integrating metabolic models with constraints derived from experimental data. BMC Syst. Biol. 8, 123.
Castillo, T., Ramos, J.L., Rodríguez-Herva, J.J., Fuhrer, T., Sauer, U., Duque, E., 2007. Convergent peripheral pathways catalyze initial glucose catabolism in *Pseudomonas putida*: genomic and flux analysis. J. Bacteriol. 189, 5142–5152.
Chao, G., Shen, J., Tseng, C.P., Park, S.J., Gunsalus, R.P., 1997. Aerobic regulation of isocitrate dehydrogenase gene (icd) expression in *Escherichia coli* by the arcA and fnr gene products. J. Bacteriol. 179 (13), 4299–4304.
Chokkathukalam, A., Kim, D.H., Barrett, M.P., Breitling, R., Creek, D.J., 2014. Stable isotope-labeling studies in metabolomics: new insights into structure and dynamics of metabolic networks. Bioanalysis 6 (4), 511–524.
Conway, T., 1992. The Entner-Doudoroff pathway: history, physiology and molecular biology. FEMS Microbiol. Rev. 103, 1–28.
Crown, S.B., Antoniewicz, M.R., 2012. Selection of tracers for ^{13}C-metabolic flux analysis using elementary metabolite units (EMU) basis vector methodology. Metab. Eng. 14, 150–161.
Crown, S.B., Long, C.P., Antoniewicz, M.R., 2016. Optimal tracers for parallel labeling experiments and ^{13}C metabolic flux analysis. A new precision synergy scoring system. Metab. Eng. 38, 10–18.
Dandekar, T., Fieselmann, A., Popp, J., Hensel, M., 2012. *Salmonella enterica*: a surprisingly well-adapted intracellular lifestyle. Front. Microbiol. 3 (164), 1–11.
Dandekar, T., Fieselmann, A., Fischer, E., Popp, J., Hensel, M., Noster, J., 2015. *Salmonella* – how a metabolic generalist adopts an intracellular lifestyle during infection. Front. Cell. Infect. Microbiol. 4 (191), 1–11.
Dauner, M., Sonderegger, M., Hochuli, M., Szyperski, T., Wüthrich, K., Hohmann, H.P., Sauer, U., Bailey, J.E., 2002. Intracellular carbon fluxes in riboflavin-producing *Bacillus subtilis* during growth on two-carbon substrate mixtures. Appl. Environ. Microbiol. 68 (4), 1760–1771.
Dauner, M., Sauer, U., 2001. Stoichiometric growth model for riboflavin-producing *Bacillus* subtilis. Biotechnol. Bioeng. 76 (2), 132–143.
Diacovich, L., Lorenzi, L., Tomassetti, M., Méresse, S., Gramajo, H., 2017. The infectious intracellular lifestyle of *Salmonella enterica* relies on the adaptation to nutritional conditions within the Salmonella-containing vacuole. Virulence 8 (6), 975–992.
Driessen, M., Postma, P.W., Van Dam, K., 1987. Energetics of glucose uptake in *Salmonella typhimurium*. Arch. Microbiol. 146, 358–361.
Enos-Berlage, J.L., Downs, D.M., 1999. Biosynthesis of the pyrimidine moiety of thiamine independent of the PurF enzyme (phosphoribosylpyrophosphate amidotransferase) in *Salmonella typhimurium*: incorporation of stable isotope-labeled glycine and formate. J. Bacteriol. 181, 841–848.
Eriksson, S., Lucchini, S., Thompson, A., Rhen, M., Hinton, J.C.D., 2003. Unravelling the biology of macrophage infection by gene expression profiling of intracellular *Salmonella enterica*. Mol. Microbiol. 47 (1), 103–118.
Feist, A.M., Henry, C.S., Reed, J.L., Krummenacker, M., Karp, P.D., Broadbelt, L.J., Hatzimanikatis, V., Palsson, B.Ø., 2007. A genome-scale metabolic reconstruction for *Escherichia coli* K-12 MG1655 that accounts for 1260 ORFs and thermodynamic information. Mol. Syst. Biol. 3, 121.
Fischer, E., Sauer, U., 2003. A novel metabolic cycle catalyzes glucose oxidation and anaplerosis in hungry *Escherichia coli*. J. Biol. Chem. 278 (47), 46446–46451.
Flamholza, A., Noora, E., Bar-Evena, A., Liebermeistera, W., Miloa, R., 2013. Glycolytic strategy as a tradeoff between energy yield and protein cost. PNAS 110 (24), 10039–10044.
Forbes, N.S., 2010. Engineering the perfect (bacterial) cancer therapy. Nat. Rev. Cancer 10 (11), 785–794.
Fuhrer, T., Fischer, E., Sauer, U., 2005. Experimental identification and quantification of glucose metabolism in seven bacterial species. J. Bacteriol. 187 (5), 1581–1590.
Gotz, A., Eylert, E., Eisenreich, W., Goebel, W., 2010. Carbon metabolism of enterobacterial human pathogens growing in epithelial colorectal adenocarcinoma (Caco-2) cells. PLoS One 5 (5), e10586.
Hartman, H.B., Fell, D.A., Rossell, S., Jensen, P.R., Woodward, M.J., Thorndahl, L., Jelsback, L., Olsen, J.E., Raghunathan, A., Daefler, S., Poolman, M.G., 2014. Identification of potential drug targets in *Salmonella enterics v. typhimurium* using metabolic modeling and experimental validation. Microbiology 160, 1252–1266.
Haverkorn van Rijsewijk, B.R.B., Nanchen, A., Nallet, S., Kleijn, R.J., Sauer, U., 2011. Large-scale 13C-flux analysis reveals distinct transcriptional control of respiratory and fermentative metabolism in *Escherichia coli*. Mol. Bio Syst. 7, 477.
Heimann, D.M., Rosenberg, S.A., 2003. Continuous intravenous administration of live genetically modified *Salmonella typhimurium* in patients with metastatic melanoma. J. Immunother. 26 (2), 179–180.
Hollinshead, W.D., Henson, W.R., Abernathy, M., Moon, T.S., Tang, Y.J., 2015. Rapid metabolic analysis of *Rhodococcus opacus* PD630 via parallel ^{13}C Metabolite Fingerprinting. Biotechnol. Bioeng. 113 (1), 91–100.
Jahn, S., Haverkorn van Rijsewijk, B.R.B., Sauer, U., Bettenbrock, K., 2013. A role for EIIANtr in controlling fluxes in the central metabolism of *E. coli* K12. Biochim. Biophys. Acta 1833, 2879–2889.
Jeong, B.Y., Wittmann, C., Kato, T., Park, E.Y., 2014. Comparative metabolic flux analysis of an *Ashbyagossypii* wild-type strain and a high riboflavin-producing mutant strain. J. Biosci. Bioeng. 119 (1), 101–106.
Kaufmann, S., Roupach, B., Finlay, B., 2001. Introduction: microbiology and immunology: lessons learned from *Salmonella*. Microbes Infect. 3, 1177–1181.
Kayser, A., Weber, J., Hecht, V., Rinas, U., 2008. Metabolic flux analysis of *Escherichia coli* in glucose-limited continuous culture. J. Ind. Microbiol. Biotechnol. 35 (6), 611–618.
Kiefer, P., Heinzle, E., Zelder, O., Wittmann, C., 2004. Comparative metabolic flux analysis of lysine-producing *Corynebacterium glutamicum* cultured on glucose or fructose. Appl. Environ. Microbiol. 70 (1), 229–239.
Kildegaard, K.R., Jensen, N.B., Schneider, K., Czarnotta, E., Özdemir, E., Klein, T., Maury, J., Ebert, B.E., Christensen, H.B., Chen, Y., Kim, I.I.-K., Ebert, M.J., Blank, L.M., Forster, J., Nielsen, J., Borodina, I., 2016. Engineering and systems-level analysis of *Saccharomyces cerevisiae* for production of 3-hydroxypropionic acid via malonyl-CoA reductase-dependent pathway. Microb. Cell Fact. 15, 53.
Fountoulakis, M., Lahm, H.W., 1998. Hydrolysis and amino acid composition analysis of proteins. J. Chromatogr. A 826, 109–134.
Kong, W., Clark-Curtis, J., Curtiss III, R., 2013. Utilizing *Salmonella* for antigen delivery: the aims and benefits of bacterial delivery vaccination. Expert Rev. Vaccin. 12 (4), 345–347.
Kothari, S., Kim, J.A., Kothari, N., Jones, C., Choe, W.S., Carbis, R., 2014. Purification of O-specific polysaccharide from lipopolysaccharide produced by *Salmonella* enteric serovar Paratyphi A. Vaccine 32 (21), 2457–2462.
Leighty, R.W., Antoniewicz, M.R., 2012. Parallel labeling experiments with [U-^{13}C] glucose validate *E. coli* metabolic network model for ^{13}C metabolic flux analysis. Metab. Eng. 14, 533–541.
Lewis, N.E., Hixson, K.K., Conrad, T.M., Lerman, J.A., Charusanti, P., Polpitiya, A.D., Adkins, J.N., Schramm, G., Purvine, S.O., Lopez-Ferrer, D., Weitz, K.K., Eils, R., Konig, R., Smith, R.D., Palsson, B.Ø., 2010. Omic data from evolved *E. coli* are consistent with computed optimal growth from genome-scale models. Mol. Syst. Biol. 6, 390.
Liu, M., Ding, Y., Chen, H., Zhao, Z., Liu, H., Xian, M., Zhao, G., 2017. Improving the production of acetyl-CoA-derived chemicals in *Escherichia coli* BL21 (DE3) through *iclR* and *arcA* deletion. BMC Microbiol. 17 (10).
Maeda, K., Okahashi, N., Toya, Y., Matsuda, F., Shimizu, H., 2016. Investigation of useful carbon tracers for ^{13}C-metabolic flux analysis of *Escherichia coli* by considering five experimentally determined flux distributions. Metab. Eng. Commun. 3, 187–195.
Mairinger, T., Wegscheider, W., Peña, D.A., Steiger, M.G., Koellensperger, G., Zanghellini, J., Hann, S., 2018. Comprehensive assessment of measurement uncertainty in ^{13}C-based metabolic flux experiments. Anal. Bioanal. Chem. 410, 3337–3348.
Millard, P., Letisse, F., Sokol, S., Portais, J.C., 2012. IsoCor: correcting MS data in isotope labeling experiments. Bioinformatics 28, 1294–1296.
Nanchen, A., Fuhrer, T., Sauer, U., 2007. Determination of Metabolic Flux Ratios from^{13}C Experiments and Gas Chromatography – Mass Spectrometry Data. Methods in Molecular Biology, vol. 358: Metabolomics: Methods and Protocols. Humana Press Inc., New Jersey.
Niu, H., Chen, Y., Yao, S., Liu, L., Yang, C., Li, B., Liu, D., Xie, J., Chen, X., Wu, J., Ying, H., 2013. Metabolic flux analysis of Arthrobacter sp. CGMCC 3584 for cAMP production based on ^{13}C tracer experiments and gas chromatography–mass spectrometry. J. Biotechnol. 168 (4), 355–361.
Oliveira, B.H., Silva, M.R., Braga, C.J.M., Massis, L.M., Ferreira, L.C.S., Crogio-Almeida, M.E., Takagi, M., 2011. Production of native flagellin from *Salmonella typhimurium* in a bioreactor and purification by tangential ultrafiltration. Braz. J. Chem. Eng. 28 (4), 575–584.
Pereira, R., Nielsen, J., Rocha, I., 2016. Improving the flux distributions simulated with genome-scale metabolic models of *Saccharomyces cerevisiae*. Metab. Eng. Commun. 3, 153–156.
Phue, J.N., Noronha, S.B., Hattacharyya, R., Wolfe, A.J., Shiloach, J., 2005. Glucose metabolism at high density growth of *E. coli* B *and E. coli* K: differences in metabolic pathways are responsible for efficient glucose utilization in *E. coli* B as determined by microarrays and Northern blot analyses. Biotechnol. Bioeng. 90 (7), 805–820.
Quek, L.E., Wittmann, C., Nielsen, L.K., Kromer, J.O., 2009. OpenFLUX: efficient modeling software for 13C-based metabolic flux analysis. Microb. Cell Fact. 8, 25.
Quek, L.E., Nielsen, L.K., 2014. Steady-State13C Fluxomics Using OpenFLUX. Methods in Molecular Biology, vol. 1191: Metabolic Flux Analysis: Methods and Protocols. Springer Science, New York.
Raghunathan, A., Reed, J., Shin, S., Palsson, B., Daefler, S., 2009. Constraint-based analysis of metabolic capacity of *Salmonella typhimurium* during host-pathogen interaction. BMC Syst. Biol. 3 (38), 1–16.
Rocha, I., Maia, P., Evangelista, P., Vilaça, P., Soares, S., Pinto, J.P., Nielsen, J., Patil, K.R., Ferreira, E.C., Rocha, M., 2010. OptFlux: an open-source software platform for *in silico* metabolic engineering. BMC Syst. Biol. 4, 45.
Russel, J.B., Cook, G.M., 1995. Energetics of bacterial growth: balance of anabolic and catabolic reactions. Microbiol. Rev. 59 (1), 48–62.
Santos, S., Rocha, I., 2016. Estimation of biomass composition from genomic and transcriptomic information. J. Int. Bioinform. 13 (2), 285.
Santos S., Rocha I., 2018. Origin and impact of biomass composition in genome-scale models predictions (submitted for publication).
Sargo, C.R., Campani, G., Silva, G.G., Giordano, R.C., Silva, A.J., Zangirolami, T.C., Correia, D.M., Ferreira, E.C., Rocha, I., 2015. *Salmonella typhimurium* and *Escherichia coli* dissimilarity: closely related bacteria with distinct metabolic profiles. Biotechnol. Prog. 31 (5), 1217–1225.
Schatschneider, S., Huber, C., Neuweger, H., Watt, T.F., Pu¨hler, A., Eisenreich, W., Wittmann, C., Niehaus, K., Vorho¨lter, J.F., 2014. Metabolic flux pattern of glucose utilization by *Xanthomonas campestris pv. campestris*: prevalent role of the Entner–Doudoroff pathway and minor fluxes through the pentose phosphate pathway and glycolysis. Mol. BioSyst. 10, 2663–2676.
Silva, A.J., Zangirolami, T.C., Novo, M.T.M., Giordano, R.C., Martins, E.A.L., 2014. Live bacterial vaccine vectors: an overview. Braz. J. Microbiol. 45 (4), 1117–1129.
Shupletsov, M.S., Golubeva, L.I., Rubina, S.S., Podvyaznikov, D.A., Iwatani, S., Mashko, S.V., 2014. OpenFLUX2: ^{13}C-MFA modeling software package adjusted for the comprehensive analysis of single and parallel labeling experiments. Microb. Cell Fact. 13, 152.
Smart, K.F., Aggio, R.B.M., Houtte, J.R.V., Villas-Bôas, S.G., 2010. Analytical platform for metabolome analysis of microbial cells using methyl chloroformate derivatization followed by gas chromatography-mass spectrometry. Nat. Protoc. 5, 1709–1729.
Stephanopoulos, G.N., Aristidou, A.A., Nielsen, J., 1998. Metabolic Engineering Principles

and Methodologies. Academic Press, San Diego.
Tao, Y., Liu, D., Yan, X., Zhou, Z., Lee, J.K., Yang, C., 2012. Network identification and flux quantification of glucose metabolism in *Rhodobacter sphaeroides* under photo-heterotrophic H_2-producing conditions. J. Bacteriol. 194, 274–283.
Thiele, I., Hyduke, D.R., Steeb, B., Fankam, G., Allen, D.K., Bazzani, S., Charusanti, P., Chen, F., Fleming, R.M.T., Hsiung, C.A., Keersmaecker, S.C.J., Liao, Y., Marchal, K., Mo, M.L., Ozdemir, E., Raghunathan, A., Reed, J.L., Shin, S., Sigurbjornsd_ottir, S., Steinmann, J., Sudarsan, S., Swainston, N., Thijs, I.M., Zengler, K., Palsson, B.Ø., Adkins, J.N., Bumann, D., 2011. A community effort towards a knowledge-base and mathematical model of the human pathogen *Salmonella typhimurium*LT2. BMC Syst. Biol. 5, 1–9.
Toya, Y., Ishii, N., Nakahigashi, K., Hirasawa, T., Soga, T., Tomita, M., Shimizu, K., 2010. ^{13}C-metabolic flux analysis for batch culture of *Escherichia coli* and its *pyk* and *pgi* gene knockout mutants based on mass isotopomer distribution of intracellular metabolites. Biotechnol. Prog. 26 (4), 975–992.
Valgepea, K., Adamberg, K., Vilu, R., 2011.. Decrease of energy spilling in *Escherichia coli* continuous cultures with rising specific growth rate and carbon wasting. BMC Syst. Biol. 5 (106), 1–11.
Villas-Bôas, S.G., Delicado, D.G., Akesson, M., Nielsen, J., 2003. Simultaneous analysis of amino and nonamino organic acids as methyl chloroformate derivatives using gas chromatography-mass spectrometry. Anal. Biochem. 322, 134–138.
Waegeman, H., Maertens, J., Beauprez, J., De Mey, M., Soetaert, W., 2012. Effect of iclR and arcA deletions on physiology and metabolic fluxes in *Escherichia coli* BL21(DE3). Biotechnol. Lett. 34 (2), 329–337.
Wilson, R.B., Malloy, S.R., 1987. Isolation and characterization of S*almonella typhimurium* glyoxylate shunt mutants. J. Bacteriol. 169 (7), 3029–3034.
Wittmann, C., 2007. Fluxome analysis using GC-MS. Microb. Cell Fact. 6, 1–17.
Wolfe, A.J., 2005. The acetate switch. Microbiol. Mol. Biol. Rev. 69 (1), 12–50.
Xie, L., Lee, S.A., Hanel, B.M., Eiteman, M.A., Altman, E., 2001. Anaerobic fermentation of *Salmonella typhimurium* with and without pyruvate carboxylase. Biotechnol. Lett. 23, 111–117.
Zamboni, N., Fendt, S.M., Rühl, M., Sauer, U., 2009. ^{13}C –based metabolic fluxanalysis. Nat. Prot. 4 (6), 878–892.